Wave equation vector migration for subsalt VSP imaging and interpretation

Denis Kiyashchenko, Wim Mulder and Jorge Lopez, Shell International Exploration and Production

SUMMARY

Interpretation of subsalt VSP data is a challenge due to low fold, uneven illumination, and the resulting presence of a large amount of migration artifacts. We propose a wave equation vector migration algoritm (VWEM) to exploit the potential of multi-component VSP surveys for imaging in complex subsalt environments. The algorithm naturally takes into account multi-pathing and is designed to enhance true events in VSP images. We also propose a noise imaging algorithm that enhances noise and suppresses true events to consistently characterize migration noise in VSP images. Joint interpretation of vector and noise images enables clear identification of true and false events. The approach was successfully applied to a 3D VSP acquired in the Gulf of Mexico in order to clarify the subsalt scenario.

INTRODUCTION

Conventionally, VSP data use downhole receivers to achieve better resolution than surface seismics and to acquire more detailed information about the reservoir. In subsalt imaging, VSPs may actually add substantial value by a different illumination from downhole receivers. But compared to surface seismics, VSP imaging has problems associated with low and inhomogeneously distributed fold. Artifacts at the edges of VSP images are a well-known issue, even for VSPs acquired on a flatly layered earth. Those artifacts are suppressed by stacking with sufficient fold. In subsalt exploration, the fold may not be high enough to suppress noise in the area of interest. Therefore, subsalt VSPs have substantial interpretation risks while still being attractive for evaluating the potential success of the prospect. Reducing those risks is the subject of this paper.

We propose a methodology for VSP image enhancement, noise reduction, and interpretation based on multi-component data processing. Most VSPs are acquired with multi-component sensors and these measurements intrinsically contain information about wave polarization, which is commonly used for shear wave separation and compressional wave enhancement. There are also applications for image steering. One of the basic ideas was to determine polarization from reflected wave hodogram and use it for reflection point location, see MacLeod (1994). With the size of modern VSP acquisitions, this approach is not practical. Therefore, it was proposed to modify the Kirchhoff imaging kernel to incorporate multi-component data and enhance the image around the Fresnel zone (Jackson et al., 1991; Wang, 2004). This is called vector Kirchhoff imaging. However, for subsalt environments wave equation instead of Kirchhoff migration is required to handle multi-pathing and other complex wave phenomena.

The problem of taking into account polarization in scalar wave equation migration was partially solved by Shoshitaishvili et al. (2004) and successfully used by Hornby et al. (2007) for deep water 3D VSP processing. The idea is to stack all single-component images with weights proportional to the components of the vector pointing from image location to receiver. This assumes that the medium between image point and receiver is relatively simple, which is not the case when receivers are close to a salt flank. Vector Wave Equation Migration (Kiyashchenko and Mulder, patent pending), discussed in this paper, is free of this assumption and works as well for cases with multi-pathing. Generally, vector imaging schemes lead to reduced migration smile noise and results are better than single-component images. However, the comparison of a conventional vertical-component image with a vector image will not necessarily confirm the validity of events in the image, because vector imaging only *partially* suppresses the amplitude of noise events but does not completely remove them. Here, we propose noise imaging as a counterpart to vector imaging. Ideally, noise imaging *completely* suppresses true events and boosts the noise so that it can be clearly identified. Joint analysis of vector and noise images enables advanced interpretation of VSP data. In the following sections, we will explain the concept of VWEM and demonstrate the application of the technology for a field in the Gulf of Mexico.

WAVE EQUATION VECTOR MIGRATION

Wave equation migration of 3D VSP data requires sorting to receiver gathers, as there are far fewer of them than sources. In this way, the data set is treated as a reverse VSP during migration: the sources are virtually located in the borehole and the receivers at the surface. Note that $\mathbf{x}_s$ is the true surface source position and $\mathbf{x}_r$ the true borehole receiver location; $u_j(\mathbf{x}_s,\mathbf{x}_r,t)$ denotes the multi-component data with $j=3$ corresponding to the vertical and $j=1,2$ to the horizontal components. Clearbout's (1971) imaging principle for single-receiver vertical component VSP data reads:

$$I_3(\mathbf{y},\mathbf{x}_r)=\int_{\omega_{\min}}^{\omega_{\max}} d\omega\, s(\mathbf{y},\mathbf{x}_r,\omega)u^*_{b3}(\mathbf{y},\mathbf{x}_r,\omega), \qquad (1)$$

where ω is the angular frequency, $\mathbf{y}$ the image point location, $s(\mathbf{y},\mathbf{x}_r,\omega)$ is the wave field generated by the source at $\mathbf{x}_r$, and $u_{b3}\ (\mathbf{y},\mathbf{x}_r,\omega)$ is the wave field obtained by back-propagation of reciprocal vertical component wave-field $u_3(\mathbf{x}_s,\mathbf{x}_r,\omega)$ virtually 'recorded' at the surface, so that $u_{b3}(\mathbf{y},\mathbf{x}_r,\omega)|_{\mathbf{y}=\mathbf{x}_s}=u_3(\mathbf{x}_s,\mathbf{x}_r,\omega)$. We use the following imaging condition to obtain the vector image:

$$I_V(\mathbf{y},\mathbf{x}_r)=\int_{\omega_{\min}}^{\omega_{\max}} d\omega\,\frac{1}{ik(\mathbf{y})}\left(\nabla_{\mathbf{x}_r}s(\mathbf{y},\mathbf{x}_r,\omega)\right)\cdot\mathbf{u}^*_b(\mathbf{y},\mathbf{x}_r,\omega), \quad (2)$$

with $\nabla_{\mathbf{x}_r}s$ the vector of derivatives of s with respect to the receiver location (each derivative represents a dipole source) and $\mathbf{u}_b=(u_{b1},u_{b2},u_{b3})$ with u_{bj} the back-propagation result of the component j ($j=1,2,3$). The dot denotes the scalar product and $k=\omega/c$ is the wave number with c the compressional

wave velocity. The imaging condition (2) is designed to maximize the amplitude of the image at true reflector locations. For a single-valued high-frequency source field, the ray-theoretical approximation $s'_{x_{rj}} \approx ikr_j s$ is valid, with r_j being the components of the unit ray vector at $\mathbf{x}_r$ for the ray connecting the image point to the receiver. Under this assumption, the resulting image $I_V \approx r_1 I_1 + r_2 I_2 + r_3 I_3$ is the same as in Shoshitaishvili et al. (2004). If Kirchhoff migration is used to compute I_j, then this result turns into Kirchhoff vector imaging (Wang, 2004):

$$I_{VK} = \sum_{j=1}^{3} r_j I_j = \sum_{\mathbf{x}_s} \sum_{j=1}^{3} r_j u_j \big(\mathbf{x}_s, \mathbf{x}_r, \tau(\mathbf{x}_s, \mathbf{y}) + \tau(\mathbf{x}_r, \mathbf{y})\big), \quad (3)$$

with $\tau(\mathbf{y}, \mathbf{x}_r)$ the travel time between the two points $\mathbf{y}$ and $\mathbf{x}_r$. The key difference between vector wave equation migration and the approaches above involving ray vector computations is that VWEM naturally handles multi-pathing.

NOISE IMAGING: ADVANCED INTERPRETATION

The vector Kirchhoff imaging in Eq. 3 gives a straightforward idea about the image amplitude distribution along the migration smiles. For a single shot and a simple medium, the ray theory approximation for reflected P-wave displacement is $u_j = A_j\ u(\mathbf{x}_s, \mathbf{x}_r, \tau(\mathbf{x}_s, \mathbf{y}) + \tau(\mathbf{x}_r, \mathbf{y}))$, where $\mathbf{A} = (A_1, A_2, A_3)$ is the unit polarization vector. Then the image amplitude is proportional to the scalar product $\mathbf{A} \cdot \mathbf{r} = \cos\theta$ with θ the angle between wave polarization and unit ray vector. So the amplitude is maximal at the true reflection point and less elsewhere. If we define the vector of Kirchhoff noise images

$$\mathbf{I}_{NK} = \mathbf{r} \times \mathbf{u}\big(\mathbf{x}_s, \mathbf{x}_r, \tau(\mathbf{x}_s, \mathbf{y}) + \tau(\mathbf{x}_r, \mathbf{y})\big), \quad (4)$$

its amplitude will be proportional to $\mathbf{A} \times \mathbf{r} = \sin\theta$, with $\times$ denoting the vector product. The amplitude of any noise image should be zero at the true reflector location and non-zero elsewhere, thus indicating the deviation of the unit ray vector at the receiver from the true signal polarization. The noise images for wave equation migration can be computed as:

$$\mathbf{I}_N = \int_{\omega_{\min}}^{\omega_{\max}} d\omega \frac{1}{ik(\mathbf{y})} \big(\nabla_{\mathbf{x}_r} s(\mathbf{y}, \mathbf{x}_r, \omega)\big) \times \mathbf{u}_b^*(\mathbf{y}, \mathbf{x}_r, \omega). \quad (5)$$

There are three noise images in the 3D case and just one in the 2D case. Note that the only difference between Eq. (5) and (2) is the use of the vector instead of the scalar product.

We will illustrate the joint interpretation of vector and noise images with a simple example. A synthetic vertical component zero-offset trace was generated for a medium with a reflector at 1500 m depth. The horizontal component records no signal in this case. The vector and noise images produced from this trace are shown in the left and right panels of Fig. 1, respectively. The vector image has a maximum amplitude at the true reflector location. However, in practice it would be difficult to determine the position of the reflector from this figure. On the other hand, the noise image has zero amplitude at the reflector and non-zero amplitude in the area around it. With this image, we can precisely locate the reflector because it is more sensitive than the vector image. In practice, the vector and noise images should be jointly analyzed to determine which events in the image are correct and which events are migration artifacts.

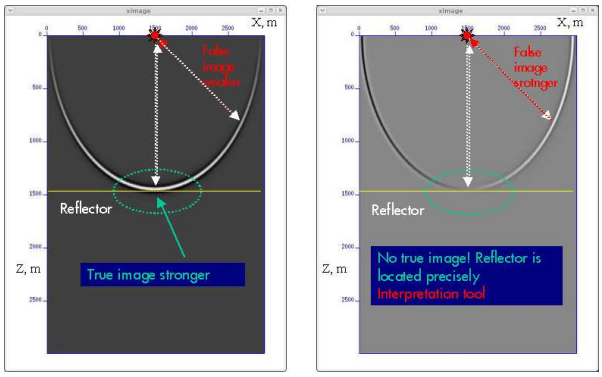

Figure 1: Vector (left) and noise (right) images for two-component zero-offset data created for a coincident source and receiver at the top of the model (red star).

VECTOR IMAGING CASE STUDY

We applied the method to VSP data from a field in the Gulf of Mexico, see Fig. 2. The basin is characterized by extensive salt tectonics. The field of interest is located below salt (indicated by the oval shape in Fig. 2), which makes mapping it with seismic data a challenge, as is evident from the cross-basin traverse in Fig. 3. The presence of two neighboring salt bodies causes significant problems in target illumination, resulting in noisy images with blind spots.

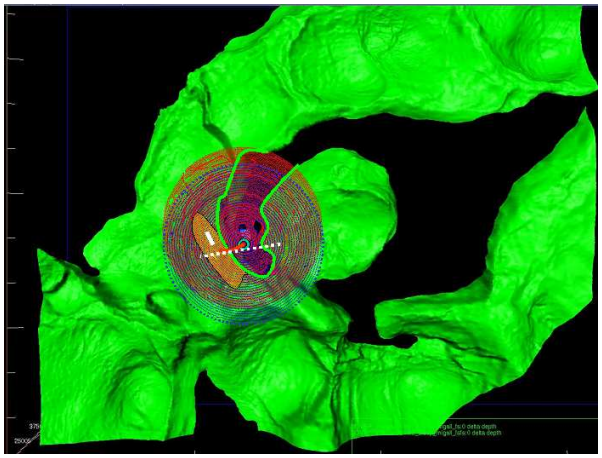

Figure 2: Map of the top of the salt. The red oval denotes the location of the field. The green line outlines the salt body edges. Blue and red dots mark the 3D VSP shots. White lines (subsalt and cross-basin) indicate the approximate traverse locations. The red line corresponds to the well trajectory.

In order to improve subsalt illumination, two large 3D VSP datasets were acquired with receivers in nearby wells. The

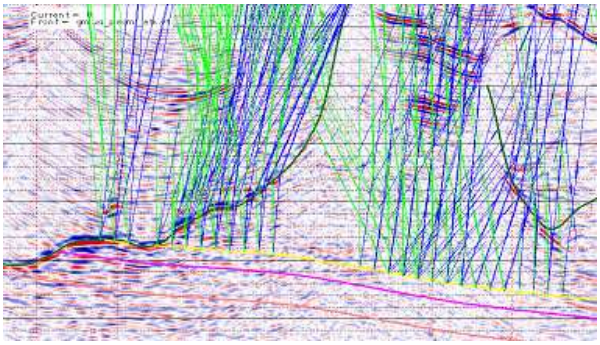

Figure 3: Surface seismic image for the cross-basin traverse. Common-offset ray tracing (offsets up to 8 km) shows large variations in target illumination due to the salt bodies.

shots for each VSP are marked by blue and red dots in Fig. 2. Here, we just show results obtained for one well (the red line in Fig. 2). Thirty receiver levels were deployed starting from 16 kft depth at 100 ft spacing. The records were quite noisy, apparently due to coupling problems. We need good vector fidelity for multi-component processing. Therefore, while checking the receiver orientation, we selected only 18 receivers that gave consistent results for different shots. As gimbaled geophones were used in this deviated well, we did not apply any orientation corrections for further processing. Prior to migration, only basic pre-processing was applied equally for all the components: a manual cut of noisy records, a band-pass filter, and an FK filter to separate upgoing waves. We used an anisotropic velocity model available for the project area. We applied a one-way propagator to redatum the sources to a certain depth above the salt and carried out reverse-time migration for the subsalt imaging. We obtained 3D volumes for the vector image, noise X image, noise Y image, and noise Z image, suitable for joint analysis. We will illustrate the analysis along two traverses.

The first traverse corresponds to the subsalt area (subsalt traverse in Fig. 2). Three VSP images (conventional vertical component, vector, and noise Y) for this short traverse are compared to one of the best surface seismic images obtained from wide azimuth OBS acquisition (OBSWAZ) in Fig. 4. The OBSWAZ image, Fig. 4a, and vertical-component VSP image, Fig. 4b, indicate the possible presence of horizontal events below the wells. The vertical-component image is fragmented due to contamination with dipping noise. The interpretation of this image requires a choice between two scenarios, horizontal or dipping, as indicated by the dashed lines in the figure. The vector image, Fig. 4c, enhances the horizontal events and suppresses the dipping ones. However, the dipping events are still present in the deeper section. The noise Y image, Fig. 4d, largely consists of dipping events and therefore convinced us that these are noise. This example of conflicting dips is typical for 3D VSPs. Vector imaging allows us to resolve this issue.

The second traverse we analyzed passes between salt bodies across the basin (cross-basin traverse in Fig. 2). Fig. 5a shows the OBSWAZ image for this traverse. The two clear events be-

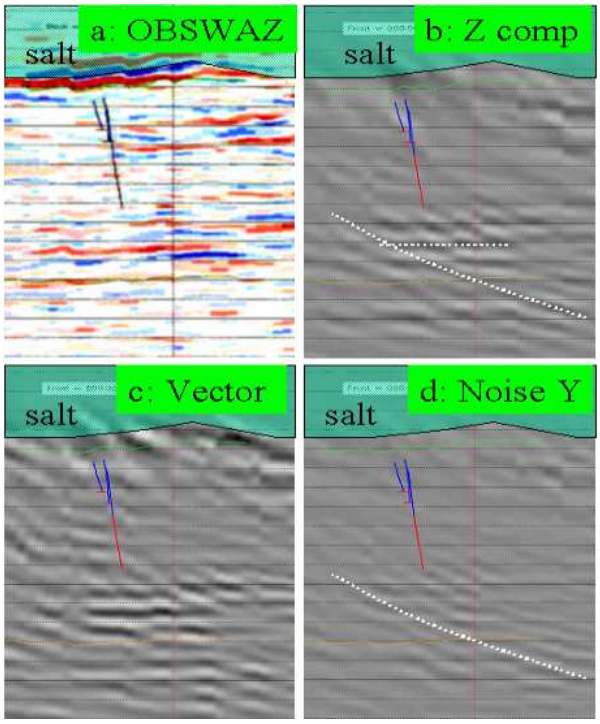

Figure 4: OBSWAZ (a) and VSP images for short subsalt traverse in Fig. 2: vertical component (b), vector image (c) and noise image Y (d). Vector and noise images resolve conflicting dips confusion.

low the salt are associated with the field reservoirs. The vertical component 3D VSP image, Fig. 5b, provides an alternative illumination of these targets and has a larger signal amplitude in the basin area. The white circle on the right indicates the events also present in the OBSWAZ image, whereas the circle on left marks the continuation of OBSWAZ events into the basin. Also, the events inside the right circle get closer to the salt than their OBSWAZ counterparts. The reverse-time migration of 3D VSP data allows us to observe events near the salt, far away from the receiver well. However, there is interference with events having conflicting dips, as indicated by the white lines. Also, there are dipping events on the right side of the image below the OBSWAZ targets. The vector image, Fig. 6a, enhances the events with smaller dips in all parts of the image. The horizontal-component energy allows us to enhance subsalt events even in the left part of the image. With lines and circles we indicate events suspected to be true. However, vector imaging does not sufficiently suppress many events with larger dips, especially in the deeper parts of the image. The noise image, Fig. 6b, consists mainly of dipping events and indicates that these do not represent a true scenario.

We note that there are events on the noise section that match the two bright events inside the right circle on the vector image. However, this does not mean that the vector image is wrong. The amplitude of those events on the noise image is much smaller than on vector image. Ideally, the noise image of true events should have zero amplitude. However, errors in

the subsalt velocity model, salt bag location, and receiver orientation may cause non-zero amplitudes of true events in the noise images. Note that vector and noise images need to be always plotted with the same amplitude scale to avoid misinterpretation. For the cross-basin traverse, we conclude that the events with small dips represent a true scenario on the basis of our vector and noise imaging method applied to this 3D VSP.

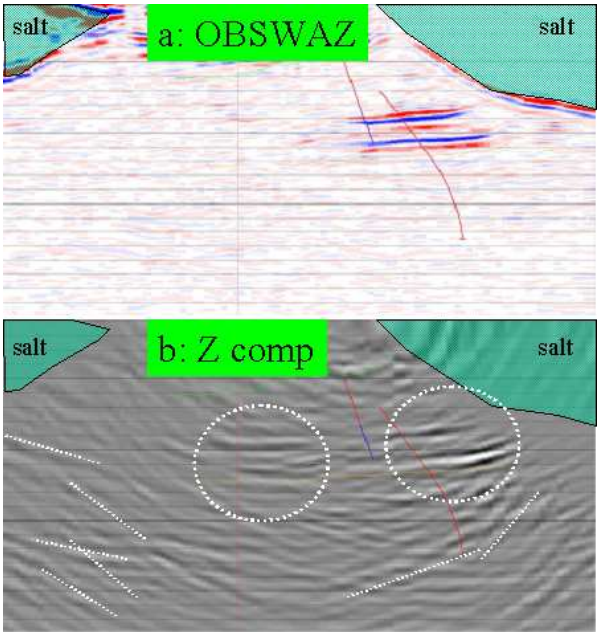

Figure 5: OBSWAZ (a) and vertical component VSP image (b) for cross-basin traverse. Note the improved subsalt imaging with 3D VSP, although conflicting dips remain.

CONCLUSIONS AND DISCUSSIONS

We proposed a vector imaging algorithm which is based on scalar wave equation migration of multi-component data. It naturally takes care of complex wave phenomena that cannot be handled by ray-based methods. Vector imaging enhances true events in the migration image by employing the polarization information intrinsically present in multi-component records. Basic pre-processing, including data cleaning, filtering, and receiver orientation corrections, suffices to prepare the data for vector imaging. It is important to do this in exactly the same way for all the components.

We also proposed a new and important extension of vector imaging, namely noise imaging, which suppresses almost completely the true events while enhancing the false ones, thus facilitating their identification. There can be many reasons for false events in VSP images: instrument noises, migration smiles, multiples, and so on. A large amount of noise is a typical problem for subsalt VSPs and it is important to identify and suppress it. The joint interpretation of vector and noise images represents a consistent approach to noise characterization. We presented an example of an application of vector and noise imaging. The vector image of 3D VSP data helps

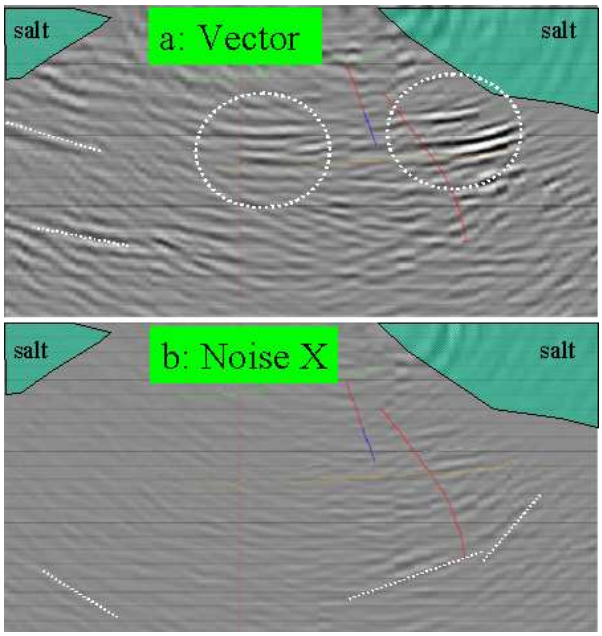

Figure 6: Vector (a) and noise (b) VSP images for cross-basin traverse. Vector migration greatly enhances subsalt image and resolves conflicting dips seen on conventional VSP processing, Fig. 5b.

to clarify subsalt interpretation and the noise images help us to understand which events are true and which are artifacts.

The interpretation based on vector and noise images may fail if the false events have the same polarization as the true ones. This might be the case when the data set is strongly contaminated with multiples that cannot be suppressed by conventional processing. However, if the polarization of a multiple is different from that of the signal, it will be suppressed by vector imaging and identified as noise. Also, vector imaging naturally suppresses shear wave reflections as their polarization is almost orthogonal to that of the compressional waves.

Usually, VSP images are interpreted jointly with surface seismics and well logs. In subsalt areas, both VSP and surface seismic images can be misleading. Using polarization information in the interpretation, as in our proposed vector and noise imaging algorithm, should reduce the risk of misinterpreting subsalt VSPs.

ACKNOWLEDGMENTS

We are grateful to our Shell colleagues Javier Ferrandis for providing his receiver orientation study results, Annemieke van den Beukel and Chris Willacy for useful discussions in the course of this work, and Mark McRae and Alexander Stopin for providing us with the data and velocity model. We thank Shell and its field co-owner BP for permission to publish this paper.

EDITED REFERENCES

Note: This reference list is a copy-edited version of the reference list submitted by the author. Reference lists for the 2009 SEG Technical Program Expanded Abstracts have been copy edited so that references provided with the online metadata for each paper will achieve a high degree of linking to cited sources that appear on the Web.

REFERENCES

Claerbout, J., 1971, Towards a unified theory of reflector mapping: Geophysics, **36**, 467–481.

Hornby, B., J. Sharp, J. Farrelly, S. Hall, and H. Sugianto, 2007, 3D VSP in the deep water Gulf of Mexico fills in subsalt shadow zone: First Break, **25**, 83–88.

Jackson, G., I. Mason, and D. Lee, 1991, Multicomponent common-receiver gather migration of single-level walkaway seismic profiles: Geophysical Prospecting, **39**, 1015–1029.

MacLeod, M., 1994, Method for delineating an anomalous geologic structure: U. S. Patent 5300929.

Shoshitaishvili, E., H. Sugianto, R. Clarke, B. Nolte, and B. Hornby, 2004, 3D multicomponent VSP processing flow for imaging beneath salt: 66th Annual Conference and Exhibition, EAGE, Extended Abstracts.

Wang, D., 2004, Vector 3C3D VSP Kirchhoff migration: 74th Annual International Meeting, SEG, Expanded Abstracts, 2458–2462.